Original Research Article

MHD Free Convection, Heat and Mass Transfer Chemical Reaction, Radiation and Heat Source or Sink over a Rotating Inclined Permeable Plate with Variable Reactive Index

ABSTRACT

MHD free convection, heat and mass transfer flow over a rotating inclined permeable plate with the influence of magnetic field, thermal radiation and chemical reaction of various order has been investigated numerically. The governing boundary-layer equations are formulated and transformed into a set of similarity equations with the help of similarity variables derived by lie group transformation. The governing equations are solved numerically using the Nactsheim-Swigert Shooting iteration technique together with the Runge-Kutta six order iteration schemes. The simulation results are presented graphically to illustrate influence of magnetic parameter (M), porosity parameter (γ), rotational parameter (R'), Grashof number (G_r), modified Grashof number (G_m), thermal conductivity parameter (T_c), Prandtl number (P_r), radiation parameter (R), heat source parameter (Q), Eckert number (E_c), Schmidt number (S_c), reaction parameter (λ) and order of chemical reaction (n) on the all fluid velocity components, temperature and concentration distribution as well as Skin-friction coefficient, Nusselt and Sherwood number at the plate.

Keywords: MHD; Inclined permeable plate; Thermal radiation; Chemical reaction;

NOMENCLATURE

B_0	Constant magnetic flux density
c	Constant depends on the properties of the fluid
C	Concentration of the fluid
C_p	Specific heat at constant pressure
D_m	Mass diffusivity
f'	Dimensionless primary velocity
g	Acceleration due to gravity
g_0	Dimensionless secondary velocity
k	Thermal conductivity
k_∞	Undisturbed thermal conductivity

26	k_0	Reaction rate
27	*K*	Permeability of the porous medium
28	*n*	Order of chemical reaction
29	*P*	Pressure distribution in the boundary layer
30	q_r	Radiative heat flux in the *y* direction
31	Q_T	Heat generation
32	Q_0	Heat source
33	*t*	Time
34	*T*	Fluid temperature
35	*U*	Uniform velocity
36	*u, v*	Velocity components along x and y axes respectively
37	x'	Dimensionless axial distance along x axis
38	**Dimensionless parameters**	
39	E_c	Eckert number
40	R'	Rotational parameter
41	G_r	Grashof number
42	G_m	Modified Grashof number
43	*M*	Magnetic parameter
44	P_r	Prandtl number
45	*Q*	Heat source parameter
46	*R*	Radiation parameter
47	S_c	Schmidt number
48	T_c	Thermal conductivity parameter
49	γ	Permeability of the porous medium
50	λ	Reaction parameter
51		
52	**Greek Symbols**	
53	υ	Kinematic viscosity of the fluid
54	μ	Dynamic viscosity of the fluid
55	σ	Electrical conductivity

σ_0	Constant electrical conductivity
σ_s	Stefan-Boltzmann constant
ρ	Density of the fluid
α	Thermal diffusivity
$\alpha_1 - \alpha_6$	Arbitrary real number
β	Inclination angle
β_T	Thermal expansion coefficient
β_C	Concentration expansion coefficient
κ^*	Mean absorption coefficient
ε	Parameter of the group
ψ	Stream function
η	Similarity variable
θ	Dimensionless temperature
φ	Dimensionless concentration
Ω	Angular velocity of the plate

Subscripts

w	Condition of the wall
∞	Condition of the free steam

1. INTRODUCTION

Coupled heat and mass transfer problems in the presence of chemical reactions are of importance in many processes and have, therefore, received considerable amount of attention of researchers in recent years. Chemical reactions can occur in processes such as drying, distribution of temperature and moisture over agricultural fields and groves of fruit trees, damage of crops due to freezing, evaporation at the surface of a water body, energy transfer in a wet cooling tower and flow in a desert cooler. Chemical reactions are classified as either homogeneous or heterogeneous processes. A homogeneous reaction is one that occurs uniformly throughout a given phase. On the other hand, a heterogeneous reaction takes a restricted area or within the boundary of a phase. Analysis of the transport processes and their interaction with chemical reactions is quite difficult and closely related to fluid dynamics. Chemical reaction effects on heat and mass transfer has been analyzed by many researchers over various geometries with various boundary conditions in porous and nonporous media. Symmetry groups or simply symmetries are invariant transformations that do not alter the structural form of the equation under investigation which is described by Bluman and Kumei [1]. MHD boundary layer equations for power law fluids with variable electric conductivity is studied by Helmy [2]. In the case of a scaling group of transformations, the group-invariant solutions are nothing but the well known similarity solutions which is studied by Pakdemirli and Yurusoy [3]. Symmetry groups and similarity

solutions for free convective boundary-layer problem was studied by Kalpakides and Balassas [4]. Makinde [5] investigated the effect of free convection flow with thermal radiation and mass transfer past moving vertical porous plate. Seddeek and Salem [6] investigated the Laminar mixed convection adjacent to vertical continuously stretching sheet with variable viscosity and variable thermal diffusivity.Ibrahim, Elaiw and Bakr [7] studied the effect of the chemical reaction and radiation absorption on the unsteady MHD free convection flow past a semi infinite vertical permeable moving plate with heat source and suction. El-Kabeir, El-Hakiem and Rashad [8] studied Lie group analysis of unsteady MHD three dimensional dimensional by natural convection from an inclined stretching surface saturated porous medium. Rajeswari, Jothiram and Nelson [9] studied the effect of chemical reaction, heat and mass transfer on nonlinear MHD boundary layer flow through a vertical porous surface in the presence of suction. Chandrakala [10] investigated chemical reaction effects on MHD flow past an impussively started semi-infinite vertical plate. Joneidi, Domairry and Babaelahi [11] studied analytical treatment of MHD free convective flow and mass transfer over a stretching sheet with chemical reaction. Muhaimin, Kandasamy and Hashim [12] studied the effect of chemical reaction, heat and mass transfer on nonlinear boundary layer past a porous shrinking sheet in the presence of suction. Rahman and Salahuddin [13] studied hydromagnetic heat and mass transfer flow over an inclined heated surface with variable viscosity and electric conductivity. As per standard text and works of previous researchers, the radiative flow of an electrically conducting fluid and heat and mass transfer situation arises in many practical applications such as in electrical power generation, astrophysical flows, solar power technology, space vehicle re-entry, nuclear reactors.

The objective of this study is to present a similarity analysis of boundary layer flow past a rotating inclined permeable plate with the influence of magnetic field, thermal radiation, thermal conductivity and chemical reaction of various orders.

2. MATHEMATICAL MODEL OF THE FLOW AND GOVERNING EQUATIONS

Steady two dimensional MHD heat and mass transfer flow with chemical reaction and radiation over an inclined permeable plate $y = 0$ in a rotating system under the influence of transversely applied magnetic field is considered. The *x*-axis is taken in the upward direction and *y*-axis is normal to it. Again the plate is inclined at an angle β with the *x*-axis. The flow takes place at $y \geq 0$, where *y* is the coordinate measured normal to the *x*-axis. Initially we consider the plate as well as the fluid is at rest with the same velocity $U\left(=U_{\infty}\right)$, temperature $T\left(=T_{\infty}\right)$ and concentration $C\left(=C_{\infty}\right)$. Also it is assumed that the fluid and plate is at rest after that the whole system is allowed to rotate with a constant angular velocity $R=\left(0,-\Omega,0\right)$ about the y-axis and then the temperature and species concentration of the plate are raised to $T_w\left(>T_{\infty}\right)$ and $C_w\left(>C_{\infty}\right)$ respectively, which are thereafter maintained constant, where T_w and C_w is the temperature and concentration respectively at wall and T_{∞} and C_{∞} is the temperature and concentration respectively far away from the plate.

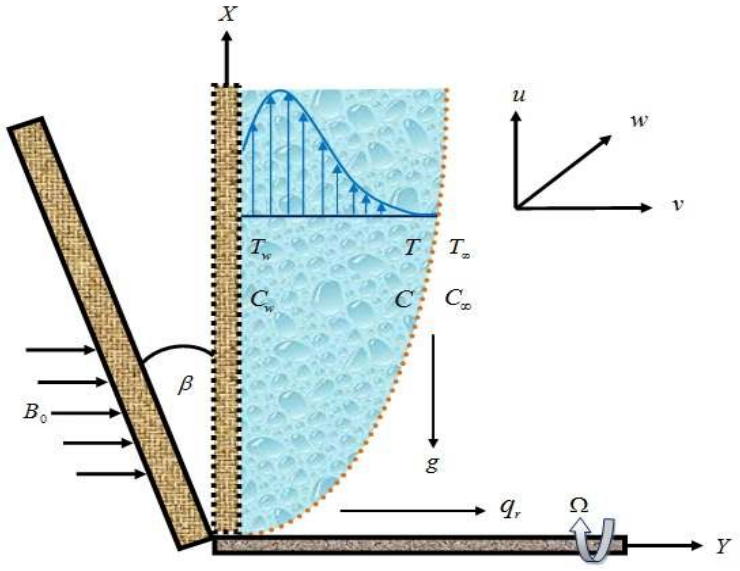

Fig. 1. Physical configuration of the flow

The electrical conductivity is assumed to vary with the velocity of the fluid and have the form [2],

$\sigma = \sigma_0 u$, σ_0 is the constant electrical conductivity.

The applied magnetic field strength is considered, as follows [13]

$$B(x) = \frac{B_0}{\sqrt{x}}$$

The temperature dependent thermal conductivity is assumed to vary linearly, as follows [6]

$$k(T) = k_\infty \left[1 + c\left(T - T_\infty\right)\right]$$

Where k_∞ is the undisturbed thermal conductivity and c is the constant depending on the properties of the fluid.

The governing equations for the continuity, momentum, energy and concentration in laminar MHD incompressible boundary-layer flow is presented as follows

$$\frac{\partial u}{\partial x} + \frac{\partial v}{\partial y} = 0 \tag{1}$$

$$u\frac{\partial u}{\partial x} + v\frac{\partial u}{\partial y} = \upsilon\frac{\partial^2 u}{\partial y^2} + 2\Omega w - \frac{\upsilon}{K}u - \frac{\sigma_0 B_0^2 u^2}{\rho x} + g\beta_T\left(T - T_\infty\right)cos\beta + g\beta_C\left(C - C_\infty\right)cos\beta \tag{2}$$

$$u\frac{\partial w}{\partial x} + v\frac{\partial w}{\partial y} = \upsilon\frac{\partial^2 w}{\partial y^2} - 2\Omega u - \frac{\upsilon}{K}w - \frac{\sigma_0 B_0^2 u w}{\rho x} \tag{3}$$

$$u\frac{\partial T}{\partial x} + v\frac{\partial T}{\partial y} = \frac{1}{\rho C_p}\frac{\partial}{\partial y}\left[k(T)\frac{\partial T}{\partial y}\right] + \frac{Q_0\left(T - T_\infty\right)}{\rho C_p} - \frac{\alpha}{k_\infty}\left(\frac{\partial q_r}{\partial y}\right) + \frac{\upsilon}{C_p}\left(\frac{\partial u}{\partial y}\right)^2 \tag{4}$$

$$u\frac{\partial C}{\partial x} + v\frac{\partial C}{\partial y} = D_m\frac{\partial^2 C}{\partial y^2} - k_0\left(C - C_\infty\right)^n \tag{5}$$

and the boundary conditions for the model is

$$\left.\begin{array}{l} u = U, v = 0, w = 0, T = T_w, C = C_w \text{ at } y = 0 \\ u \to 0, w \to 0, T \to T_\infty, C \to C_\infty \text{ as } y \to \infty \end{array}\right\} \quad (6)$$

where, U is the uniform velocity, β is the inclination angle of the plate with x-axis, C_p is the specific heat at constant pressure, $k(T)$ is the temperature dependent thermal conductivity, Q_0 is the heat source, D_m is the mass diffusivity, k_0 is the reaction rate, $k_0 > 0$ for destructive reaction, $k_0 = 0$ for no reaction and $k_0 < 0$ for generative reaction, n (integer) is the order of chemical reaction, q_r is the chemical reaction parameter, T_w and C_w is the temperature and concentration respectively at wall and T_∞ and C_∞ is the temperature and concentration respectively far away from the plate.

2.1 METHOD OF SOLUTION

Introducing the following dimensionless variables

$$x' = \frac{xU}{\upsilon}, y' = \frac{yU}{\upsilon}, u' = \frac{u}{U}, v' = \frac{v}{U}, w' = \frac{w}{U}, \theta = \frac{T - T_\infty}{T_w - T_\infty} \text{ and } \varphi = \frac{C - C_\infty}{C_w - C_\infty}$$

the following equations are obtained,

$$u = U u', v = U v', w = U w', T = T_\infty + (T_w - T_\infty)\theta \text{ and } C = C_\infty + (C_w - C_\infty)\varphi \quad (7)$$

Now, by using equation (7), the equations (1), (2), (3), (4) and (5) are transformed to

$$\frac{\partial u'}{\partial x'} + \frac{\partial v'}{\partial y'} = 0 \quad (8)$$

$$u'\frac{\partial u'}{\partial x'} + v'\frac{\partial u'}{\partial y'} = \frac{\partial^2 u'}{\partial y'^2} + 2R'w' - \gamma u' - \frac{M u'^2}{x'} + G_r \theta cos\beta + G_m \varphi cos\beta \quad (9)$$

$$u'\frac{\partial w'}{\partial x'} + v'\frac{\partial w'}{\partial y'} = \frac{\partial^2 w'}{\partial y'^2} - 2R'u' - \gamma w' - \frac{M u' w'}{x'} \quad (10)$$

$$u'\frac{\partial \theta}{\partial x'} + v'\frac{\partial \theta}{\partial y'} - \frac{1}{P_r}\left[(1 + T_c\theta + R)\frac{\partial^2 \theta}{\partial y'^2} + T_c\left(\frac{\partial \theta}{\partial y'}\right)^2\right] - Q\theta - E_c\left(\frac{\partial u}{\partial y}\right)^2 = 0 \quad (11)$$

$$u'\frac{\partial \varphi}{\partial x'} + v'\frac{\partial \varphi}{\partial y'} - \frac{1}{S_C}\frac{\partial^2 \varphi}{\partial y'^2} + \lambda\varphi^n = 0 \quad (12)$$

using equation (7), the boundary condition (6) becomes,

$$\left.\begin{array}{l} u' = 1, v' = 0, w' = 0, \theta = 1, \varphi = 1 \text{ at } y' = 0 \\ u' \to 0, w' \to 0, \theta \to 0, \varphi \to 0 \text{ as } y' \to \infty \end{array}\right\} \quad (13)$$

where,

$$R' = \frac{\Omega\upsilon}{U^2}, \gamma = \frac{\upsilon^2}{KU^2}, M = \frac{\sigma_0 B_0^2}{\rho}, G_r = \frac{g\beta_T(T_w - T_\infty)\upsilon}{U^3}, G_m = \frac{g\beta_c(C_w - C_\infty)\upsilon}{U^3}, T_c = c(T_w - T_\infty),$$

$$R = \frac{16\sigma_S T_\infty^3}{3\kappa^* k_\infty}, P_r = \frac{\upsilon}{\alpha}, Q = \frac{Q_0\upsilon}{\rho C_p U^2}, E_c = \frac{U^2}{C_p(T_w - T_\infty)}, S_c = \frac{\upsilon}{D_m} \text{ and } \lambda = \frac{k_0(C_w - C_\infty)^{n-1}\upsilon}{U^2}$$

In order to deal with the problem, we introduce the stream function ψ (since the flow is incompressible) defined by

$$u' = \frac{\partial \psi}{\partial y'}, v' = -\frac{\partial \psi}{\partial x'} \tag{14}$$

The mathematical significance of using equation (14) is that the continuity equation (8) is satisfied automatically.

By equation (14), equations (9), (10), (11) and (12) transformed as follows,

$$\frac{\partial \psi}{\partial y'}\frac{\partial^2 \psi}{\partial x' \partial y'} - \frac{\partial \psi}{\partial x'}\frac{\partial^2 \psi}{\partial y'^2} - \frac{\partial^3 \psi}{\partial y'^3} - 2R'w' + \gamma \frac{\partial \psi}{\partial y'} + \frac{M}{x'}\left(\frac{\partial \psi}{\partial y'}\right)^2 - G_r \theta cos\beta - G_m \varphi cos\beta = 0 \tag{15}$$

$$\frac{\partial \psi}{\partial y'}\frac{\partial w'}{\partial x'} - \frac{\partial \psi}{\partial x'}\frac{\partial w'}{\partial y'} - \frac{\partial^2 w'}{\partial y'^2} + 2R'\frac{\partial \psi}{\partial y'} + \gamma w' + \frac{M}{x'}\frac{\partial \psi}{\partial y'}w' = 0 \tag{16}$$

$$\frac{\partial \psi}{\partial y'}\frac{\partial \theta}{\partial x'} - \frac{\partial \psi}{\partial x'}\frac{\partial \theta}{\partial y'} - \frac{1}{P_r}\left[\left(1 + T_c\theta + R\right)\frac{\partial^2 \theta}{\partial y'^2} + T_c\left(\frac{\partial \theta}{\partial y'}\right)^2\right] - Q\theta - E_c\left(\frac{\partial^2 \psi}{\partial y'^2}\right)^2 = 0 \tag{17}$$

$$\frac{\partial \psi}{\partial y'}\frac{\partial \varphi}{\partial x'} - \frac{\partial \psi}{\partial x'}\frac{\partial \varphi}{\partial y'} - \frac{1}{S_c}\frac{\partial^2 \varphi}{\partial y'^2} + \lambda \varphi^n = 0 \tag{18}$$

and the boundary conditions (13) become,

$$\left.\begin{aligned} &\frac{\partial \psi}{\partial y'} = 1, \frac{\partial \psi}{\partial x'} = 0, w' = 0, \theta = 1, \varphi = 1 \text{ at } y' = 0 \\ &\frac{\partial \psi}{\partial y'} \to 0, w' \to 0, \theta \to 0, \varphi \to 0 \quad \text{as } y' \to \infty \end{aligned}\right\} \tag{19}$$

Finding the similarity solution of the equations (15) to (18) is equivalent to determining the invariant solutions of these equations under a particular continuous one parameter group. Introducing the simplified form of Lie-group transformations [8] namely, the scaling group of transformations

$$G_1 : x^* = x'e^{\varepsilon\alpha_1}, y^* = y'e^{\varepsilon\alpha_2}, \psi^* = \psi e^{\varepsilon\alpha_3}, w^* = w'e^{\varepsilon\alpha_4}, \theta^* = \theta e^{\varepsilon\alpha_5} \text{ and } \varphi^* = \varphi e^{\varepsilon\alpha_6} \tag{20}$$

Here, $\varepsilon(\neq 0)$ is the parameter of the group and $\alpha's$ are arbitrary real numbers whose interrelationship will be determined by our analysis. Equations (20) may be considered as a point transformation which transforms the coordinates $(x', y', \psi, w', \theta, \varphi)$ to the coordinates $(x^*, y^*, \psi^*, w^*, \theta^*, \varphi^*)$.

The system will remain invariant under the group transformation G_1, so the following relations among the exponents are obtained from equations (15) to (18),

$$\left.\begin{aligned} &\alpha_1 + 2\alpha_2 - 2\alpha_3 = 3\alpha_2 - \alpha_3 = -\alpha_4 = \alpha_2 - \alpha_3 = -\alpha_5 = -\alpha_6 \\ &\alpha_1 + \alpha_2 - \alpha_3 - \alpha_4 = 2\alpha_2 - \alpha_4 = \alpha_2 - \alpha_3 = -\alpha_4 \\ &\alpha_1 + \alpha_2 - \alpha_3 - \alpha_5 = 2\alpha_2 - \alpha_5 = 2\alpha_2 - 2\alpha_5 = 4\alpha_2 - 2\alpha_3 \\ &\alpha_1 + \alpha_2 - \alpha_3 - \alpha_6 = 2\alpha_2 - \alpha_6 = -n\alpha_6 \end{aligned}\right\} \tag{21}$$

Again, the following relations are obtained from the boundary conditions (19),

$$\left.\begin{aligned} &\alpha_2 = \alpha_3 \\ &\alpha_5 = \alpha_6 = 0 \end{aligned}\right\} \tag{22}$$

Solving the system of linear equations (21) and (22), the following relationship are obtained,

$\alpha_1 = 2\alpha_2 = 2\alpha_3, \alpha_4 = \alpha_5 = \alpha_6 = 0$

by using the above relation the equation (20) reduces to the following group of transformation

$$x^* = x'e^{2\varepsilon\alpha_2}, y^* = y'e^{\varepsilon\alpha_2}, \psi^* = \psi e^{\varepsilon\alpha_2}, w^* = w', \theta^* = \theta, \varphi^* = \varphi \quad (23)$$

expanding equation (23) by Taylor's method in powers of ε and keeping terms up to the order ε, we have

$x^* - x' = 2\varepsilon x'\alpha_2, y^* - y' = \varepsilon y'\alpha_2, \psi^* - \psi = \varepsilon\psi\alpha_2, w^* - w' = 0, \theta^* - \theta = 0, \varphi^* - \varphi = 0$

In terms of differentials

$$\frac{dx'}{2\alpha_2 x'} = \frac{dy'}{\alpha_2 y'} = \frac{d\psi}{\alpha_2\psi} = \frac{dw'}{0} = \frac{d\theta}{0} = \frac{d\varphi}{0} \quad (24)$$

Solving the equation (24) the following similarity variables are introduced,

$\eta = \frac{y'}{\sqrt{x'}}, \psi = \sqrt{x'} f(\eta), w' = g_0(\eta), \theta = \theta(\eta)$ and $\varphi = \varphi(\eta)$

By using the above mentioned variables, equations (15), (16), (17) and (18) becomes

$$f''' + \frac{1}{2} ff'' - Mf'^2 + 2R'g_0 - \gamma f' + G_r \theta cos\beta + G_m \varphi cos\beta = 0 \quad (25)$$

$$g_0'' + \frac{1}{2} fg_0' - 2R'f' - \gamma g_0 - Mf'g_0 = 0 \quad (26)$$

$$\frac{1}{P_r}(1 + T_c\theta + R)\theta'' + \frac{1}{P_r} T_c \theta'^2 + \frac{1}{2} f\theta' + Q\theta + E_c f''^2 = 0 \quad (27)$$

$$\frac{1}{S_c}\varphi'' + \frac{1}{2} f\varphi' - \lambda\varphi^n = 0 \quad (28)$$

The corresponding boundary conditions (19) become

$$\left.\begin{array}{l} f' = 1, f = 0, g_0 = 0, \theta = 1, \varphi = 1 \text{ at } \eta = 0 \\ f' \to 0, g_0 \to 0, \theta \to 0, \varphi \to 0 \text{ as } \eta \to \infty \end{array}\right\} \quad (29)$$

where primes denote differentiation with respect to η only and the parameters are defined as

$M = \frac{\sigma_0 B_0^2}{\rho}$ is the magnetic parameter

$\gamma = \frac{\upsilon^2 x'}{KU^2}$ is the porosity parameter

$R' = \frac{\Omega \upsilon x'}{U^2}$ is the rotational parameter

$G_r = \frac{g\beta_T (T_w - T_\infty)\upsilon x'}{U^3}$ is the Grashof number

$G_m = \frac{g\beta_c (C_w - C_\infty)\upsilon x'}{U^3}$ is the modified Grashof number

$T_c = c(T_w - T_\infty)$ is the thermal conductivity parameter

$P_r = \frac{\upsilon}{\alpha}$ is the Prandtl number

$R = \frac{16\sigma_s T_\infty^3}{3\kappa^* k_\infty}$ is the radiation parameter

$Q = \frac{Q_0 \upsilon}{\rho C_p U^2}$ is the heat source parameter

$E_c = \frac{U^2}{C_p\left(T_w - T_\infty\right)}$ is Eckert number

$S_c = \frac{\upsilon}{D_m}$ is the Schmidt number

$\lambda = \frac{k_0\left(C_w - C_\infty\right)^{n-1}\upsilon}{U^2}$ is the reaction parameter

and *n* (integer) is the order of chemical reaction

2.2 SKIN-FRICTION COEFFICIENTS, NUSSELT AND SHERWOOD NUMBER

The physical quantities of the skin-friction coefficients, the reduced Nusselt number and reduced Sherwood number are calculated respectively by the following equations,

$$C_f\left(R_e\right)^{\frac{1}{2}} = -f''(0) \tag{30}$$

$$C_{g_0}\left(R_e\right)^{\frac{1}{2}} = -g_0'(0) \tag{31}$$

$$N_u\left(R_e\right)^{-\frac{1}{2}} = -\theta'(0) \tag{32}$$

$$S_h\left(R_e\right)^{-\frac{1}{2}} = -\varphi'(0) \tag{33}$$

where, $R_e = \frac{Ux'}{\upsilon}$ is the Reynolds number.

3. RESULTS AND DISCUSSION

The heat and mass transfer problem associated with laminar flow past an inclined plate of a rotating system has been studied. In order to investigated the physical representation of the problem, the numerical values of primary velocity, secondary velocity, temperature and species concentration from equations (25), (26), (27) and (28) with the boundary layer have been computed for different parameters as the magnetic parameter (M), the rotational parameter (R'), the porosity parameter (γ), the Grashof number (G_r), the modified Grashof number (G_m), the radiation parameter (R), the Prandtl number (P_r), the Eckert number (E_c), the thermal conductivity parameter (T_c), the heat source parameter (Q), the Schmidt number (S_c), the reaction parameter (λ), the inclination angle (β) and the order of chemical reaction (n) respectively.

Figs. 2a and 2b show typical profiles for primary velocity (f') and secondary velocity (g_0) for different values of magnetic parameter, respectively. It is observed that as the magnetic parameter increases, the primary and secondary velocities decreases and increases respectively, where other parameters have the value $R' = Gr = Gm = \gamma = Pr = Tc = R = 0.1$, $Q = Ec = Sc = \lambda = 0.1, \beta = 60^0, n = 1$.

Figs. 3a, 3b, 3c and 3d present typical profiles for primary velocity (f'), secondary velocity (g_0), temperature (θ) and concentration (φ) for different values of rotational parameter, respectively. It is observed that as the rotational parameter increases, the primary velocity is decreasing where as the secondary velocity, temperature and concentration is increasing respectively, where other parameters have the value $M = Gr = Gm = \gamma = Pr = Tc = R = Q = Ec = Sc = 0.1,\ \lambda = 0.1, \beta = 60^0, n = 1$.

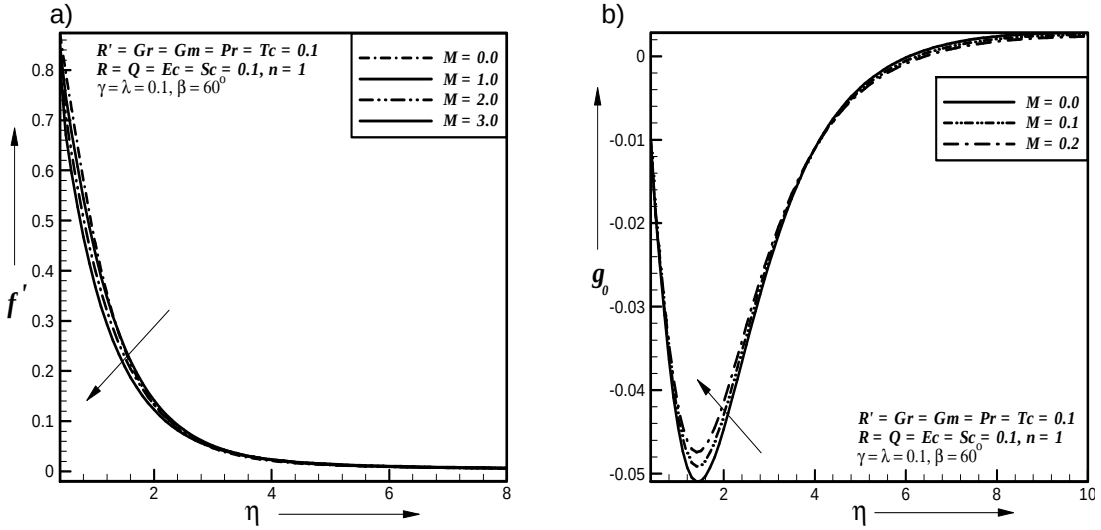

Fig. 2. Effect of magnetic parameter on a) primary velocity b) secondary velocity profiles

a) b)

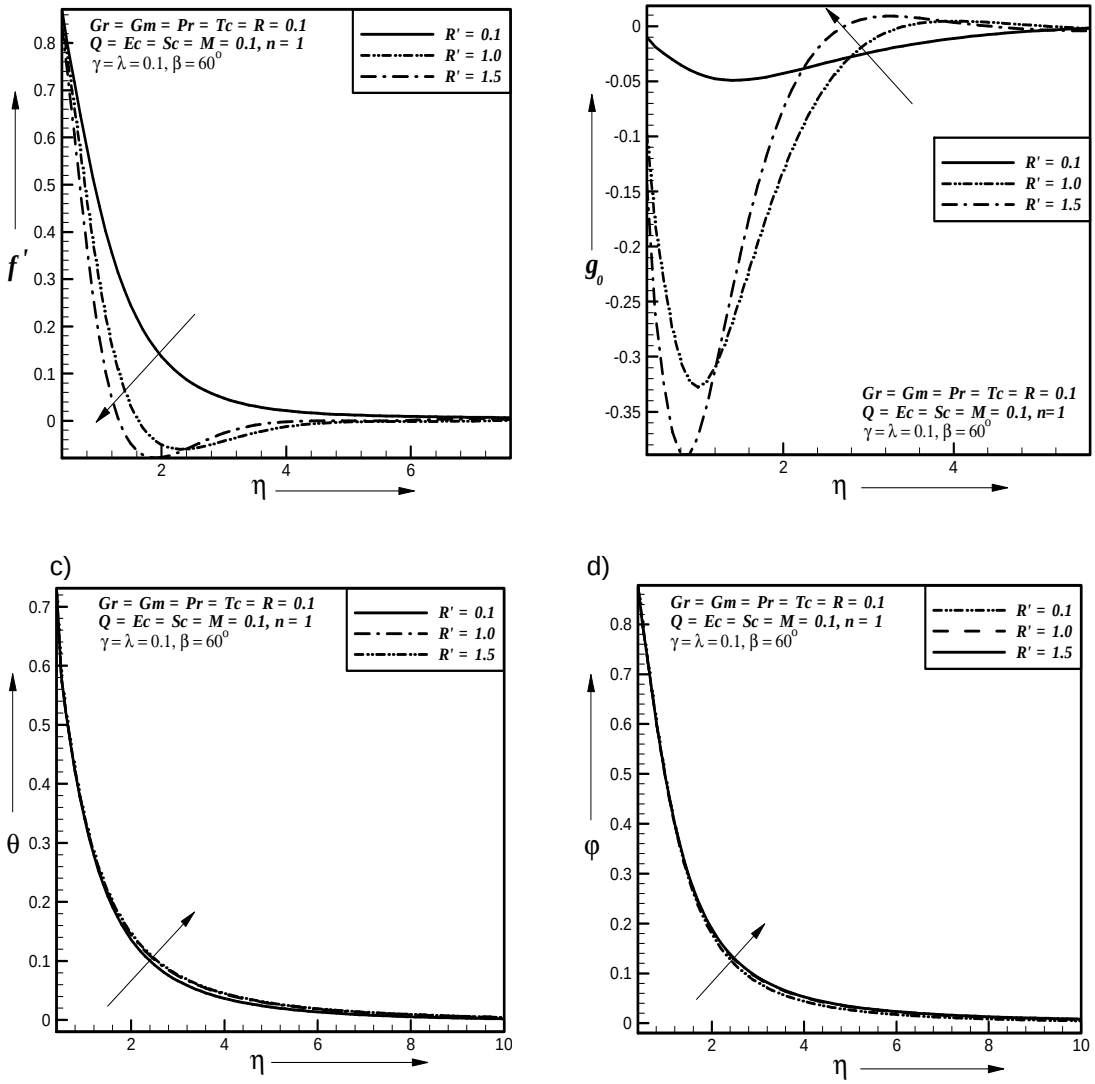

Fig. 3. Effect of rotational parameter on a) primary velocity b) secondary velocity c) temperature d) concentration profiles

Figs. 4a, 4b, 4c and 4d show typical profiles for primary velocity (f'), secondary velocity (g_0), temperature (θ) and concentration (φ) for different values of porosity parameter γ, respectively. It is observed that as the porosity parameter increases, the primary velocity decreases whereas the secondary velocity, temperature and concentration increases respectively, where other parameters have the value $M = R' = Gr = Gm = Pr = Tc = R = Q = Ec = Sc = \lambda = 0.1, \beta = 60^0, n = 1$.

a) b)

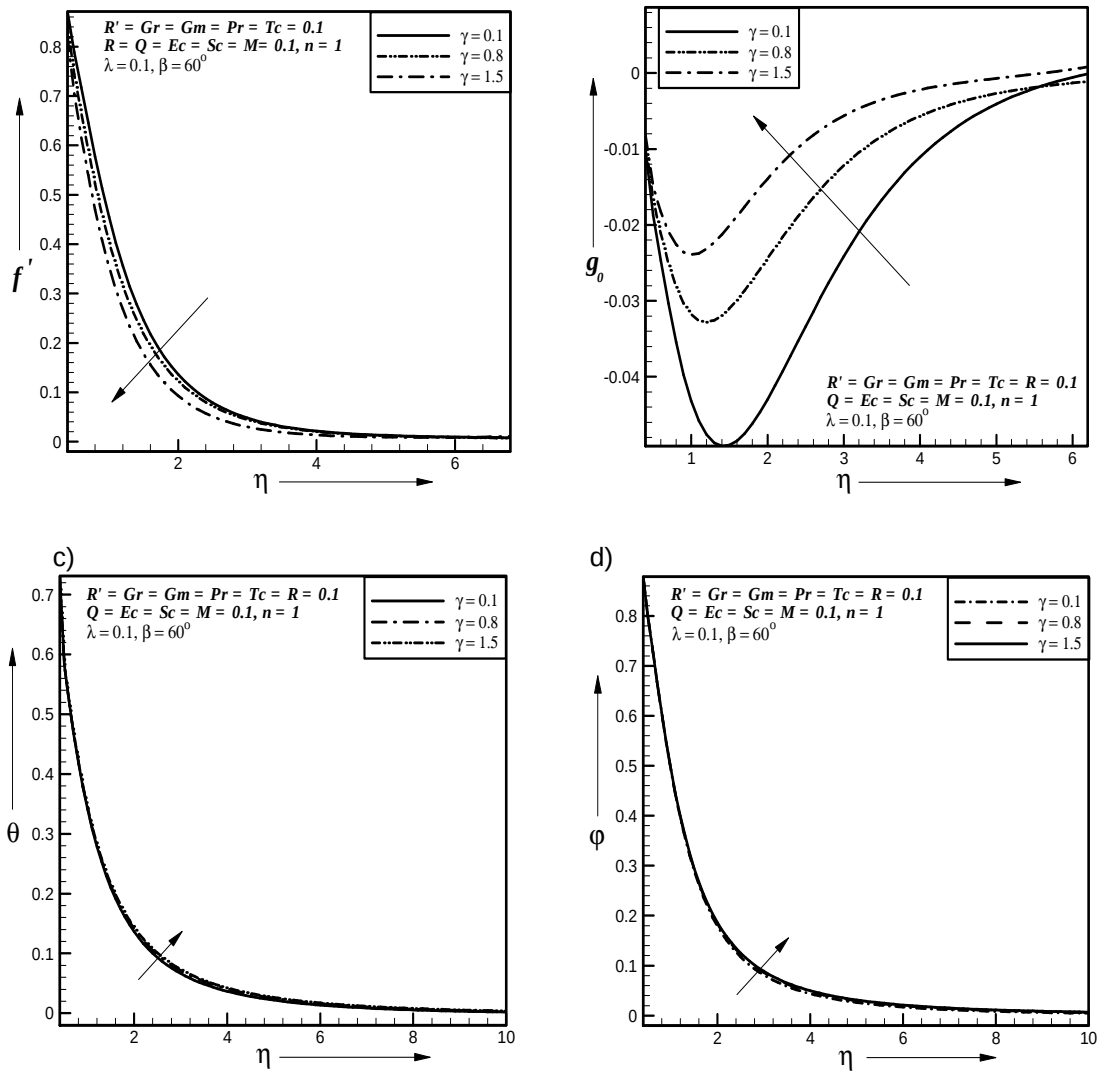

Fig. 4. Effect of porosity parameter on a) primary velocity b) secondary velocity c) temperature d) concentration profiles

Figs. 5a and 5b present typical profiles for primary velocity (f') and secondary velocity (g_0) for different values of inclination angle, respectively. It is observed that as the inclination angle increases, the primary and secondary velocities are decreasing and increasing respectively, where other parameters have the value $M = R' = Gr = Gm = \gamma = 0.1$, $Pr = Tc = R = Q = Ec = Sc = \lambda = 0.1, n = 1$.

a) b)

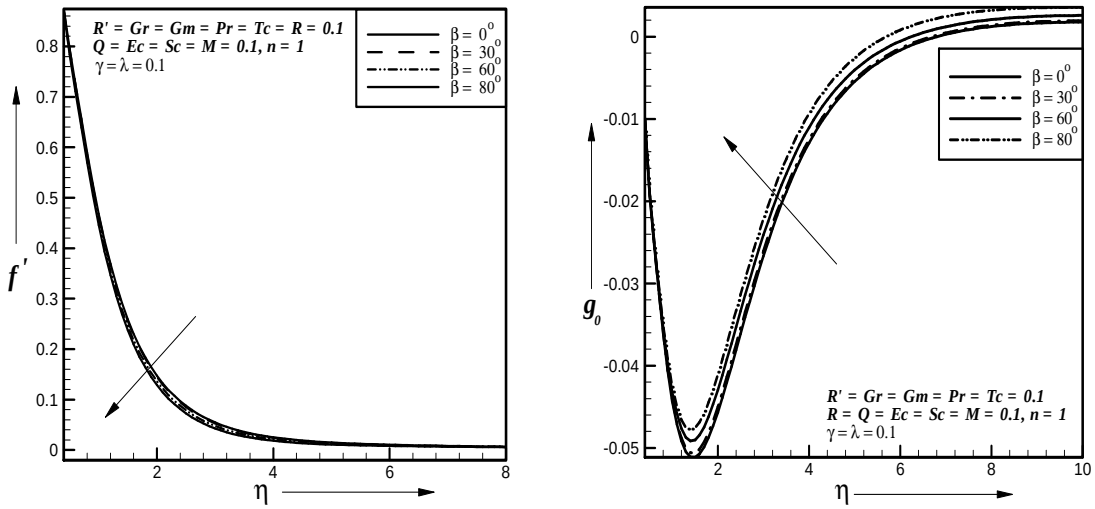

Fig. 5. Effect of inclination angle on a) primary velocity b) secondary velocity profiles

Figs. 6a, 6b and 6c present typical profiles for primary velocity (f'), secondary velocity (g_0) and temperature (θ) for different values of Grashof number, respectively. It is observed that as the Grashof number increases, the primary velocity is increasing whereas the secondary velocity and temperature is decreasing respectively, where other parameters have the value $M = R' = \gamma = Gm = Pr = Tc = R = Q = Ec = Sc = \lambda = 0.1, \beta = 60^0, n = 1$.

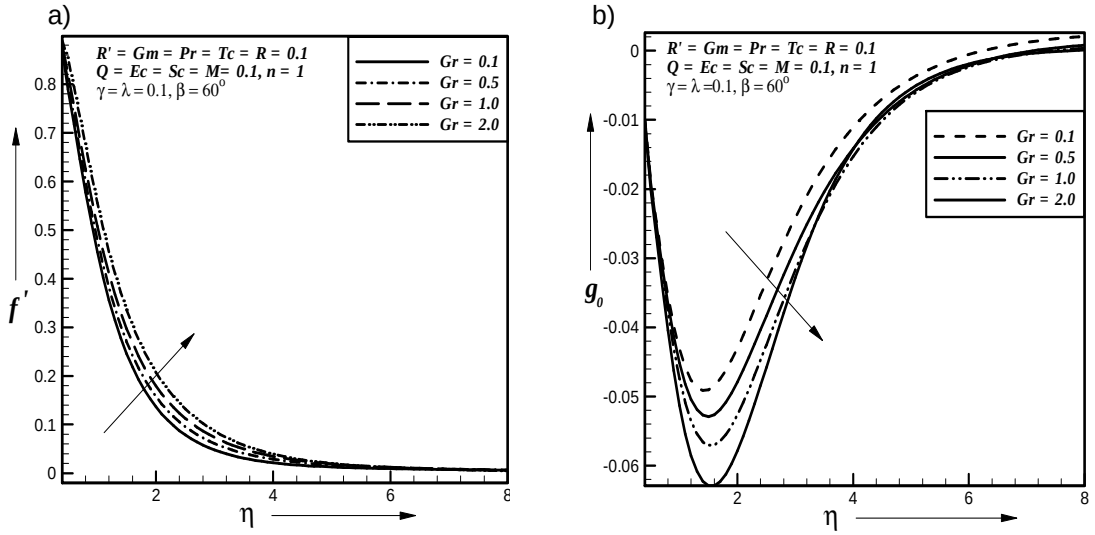

c)

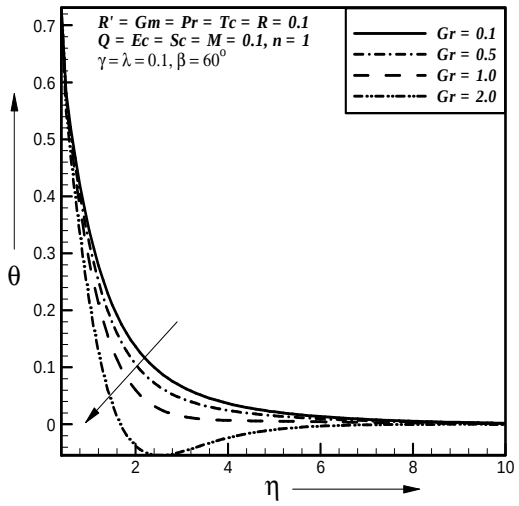

Fig. 6. Effect of Grashof number on a) primary velocity b) secondary velocity c) temperature profiles

Figs. 7a, 7b and 7c show typical profiles for primary velocity (f'), secondary velocity (g_0) and concentration (φ) for different values of modified Grashof number, respectively. It is observed that as the modified Grashof number increases, the primary velocity increases whereas the secondary velocity and concentration decreases respectively, where other parameters have the value $M = R' = \gamma = Gr = Pr = Tc = R = Q = Ec = Sc = \lambda = 0.1, \beta = 60^0$, $n = 1$.

Figs. 8a and 8b present typical profiles for primary velocity (f') and temperature (θ) for different values of Prandtl number, respectively. It is observed that as the Prandtl number increases, the primary velocity and temperature increases and decreases respectively, where other parameters have the value $M = R' = Gr = Gm = \gamma = Tc = R = Q = Ec = Sc = 0.1$, $\lambda = 0.1, \beta = 60^0, n = 1$.

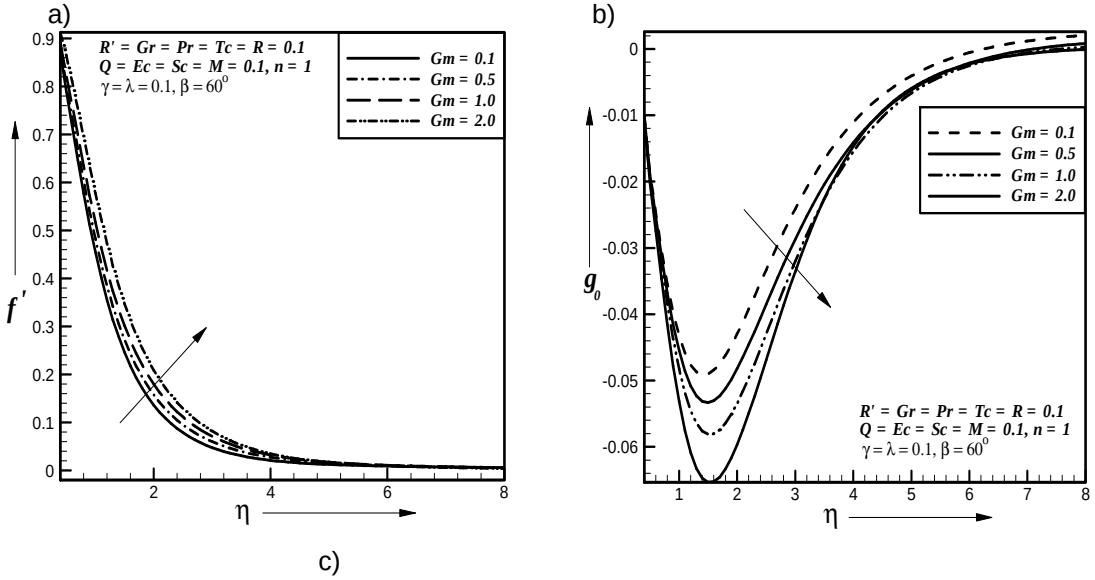

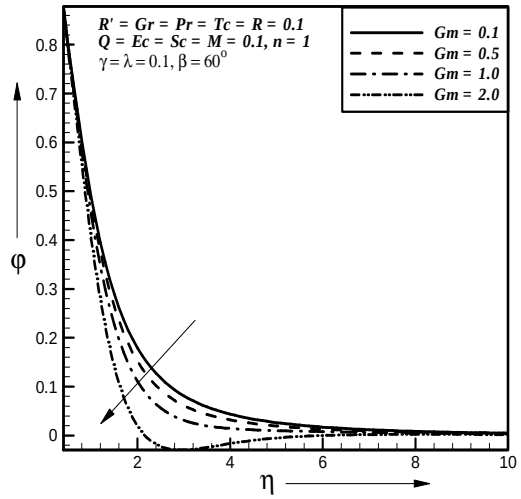

Fig. 7. Effect of modified Grashof number on a) primary velocity b) secondary velocity c) concentration profiles

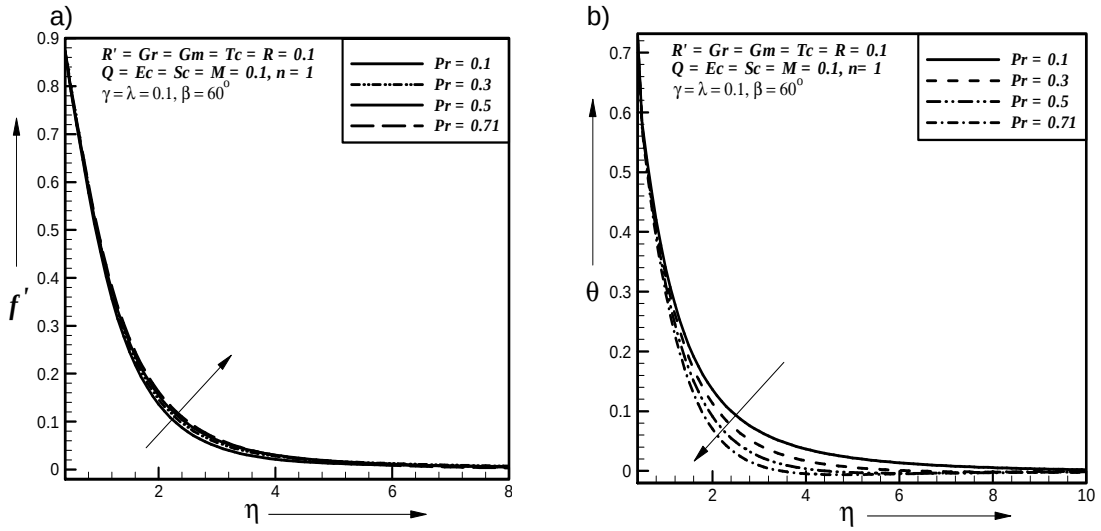

Fig. 8. Effect of Prandtl number on a) primary velocity b) temperature profiles

Fig. 9a displays typical profiles for primary velocity (f') for different values of Eckert number. It is observed that the primary velocity is increases with the increase of Eckert number, where other parameters have the value $M = Gr = Gm = \gamma = Pr = Tc = R = Q = R' = Sc = 0.1$, $\lambda = 0.1, \beta = 60^0, n = 1$.

Fig. 9b displays typical profiles for temperature (θ) for different values of Thermal conductivity parameter. It is observed that the temperature is increases with the increase of Thermal conductivity parameter, where other parameters have the values $M = Gr = Gm = \gamma = Pr = 0.1,\ Ec = R = Q = R' = Sc = \lambda = 0.1, \beta = 60^0, n = 1$.

a) b)

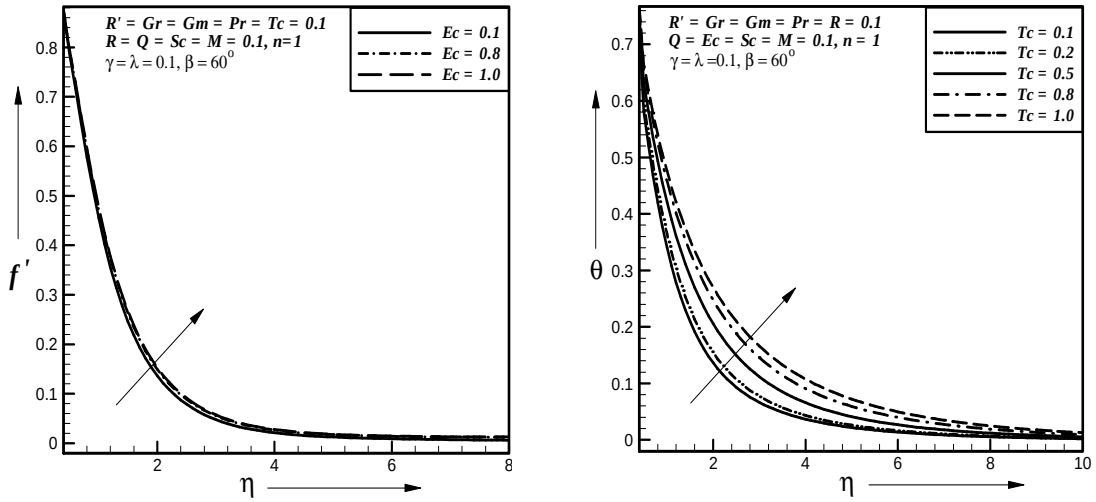

Fig. 9. Effect of a) Eckert number on primary velocity profiles b) thermal conductivity parameter on temperature profiles

Fig. 10a represents typical profiles for concentration (φ) for different values of Schmidt number Sc. It is observed that the concentration decreases with increase of Schmidt number, where other parameters have the value $M = Gr = Gm = \gamma = Pr = Ec = Q = 0.1$, $Tc = R' = R = \lambda = 0.1, \beta = 60^0, n = 1$.

Fig. 10b represents typical profiles for concentration (φ) for different values of reaction parameter λ. The no reaction $(\lambda = 0.0)$ and destructive reaction $(\lambda > 0.0)$ is studied. It is observed that the concentration decreases with the increase of reaction parameter, where other parameters have the value $M = Gr = Gm = \gamma = Pr = Ec = Q = Tc = R' = R = Sc = 0.1$, $\beta = 60^0, n = 1$.

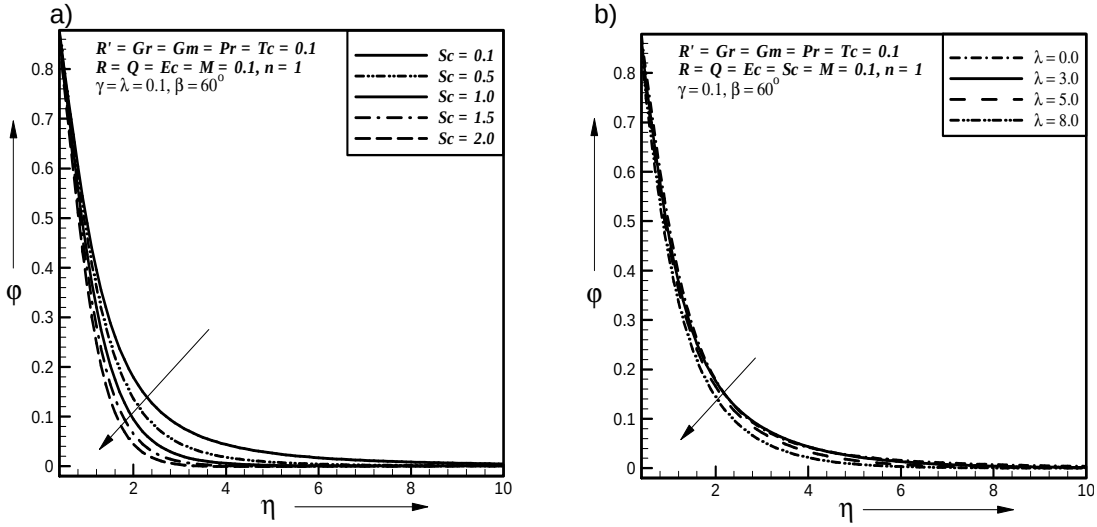

Fig. 10. Effect of a) Schmidt number on concentration profiles b) reaction parameter on concentration profiles

For the physical interest of the problem, the dimensionless skin-friction coefficient $\left(-f''\right)$ and $\left(-g_0'\right)$, the dimensionless heat transfer rate $\left(-\theta'\right)$ at the plate and the dimensionless mass transfer rate $\left(-\varphi'\right)$ at the plate are plotted against Heat source parameter $\left(Q\right)$ and illustrated in Figs. 11-19.

Figs. 11a 1nd 11b represent the primary shear stress $\left(-f''\right)$ and secondary shear stress $\left(-g_0'\right)$ which are plotted against heat source parameter $\left(Q\right)$ for different values of magnetic parameter. It is observed that the primary shear stress decreases and secondary shear stress increases with the increase of magnetic parameter, where other parameters have the value $R' = Gr = Gm = \gamma = Pr = Ec = Q = Tc = R = Sc = \lambda = 0.1, \beta = 60^0, n = 1$.

Figs. 12a and 12b represent the primary shear stress $\left(-f''\right)$ and secondary shear stress $\left(-g_0'\right)$ which are plotted against heat source parameter $\left(Q\right)$ for different values of rotational parameter. It is observed that the primary shear stress decreases and secondary shear stress increases with the increase of rotational parameter, where other parameters have the value $M = Gr = Gm = \gamma = Pr = Ec = Q = Tc = R = Sc = \lambda = 0.1, \beta = 60^0, n = 1$.

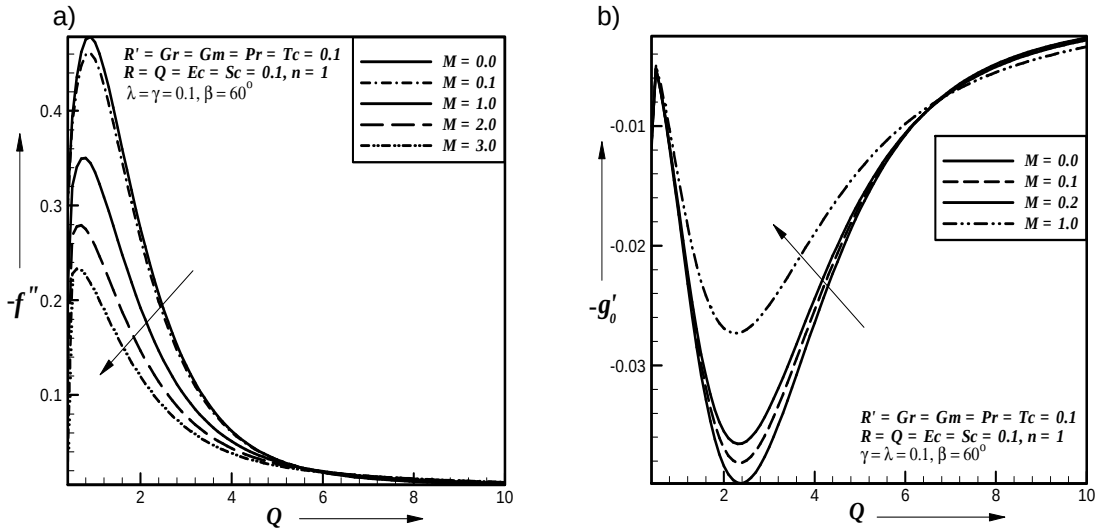

Fig. 11. Effect of magnetic parameter on a) primary shear stress b) secondary shear stress

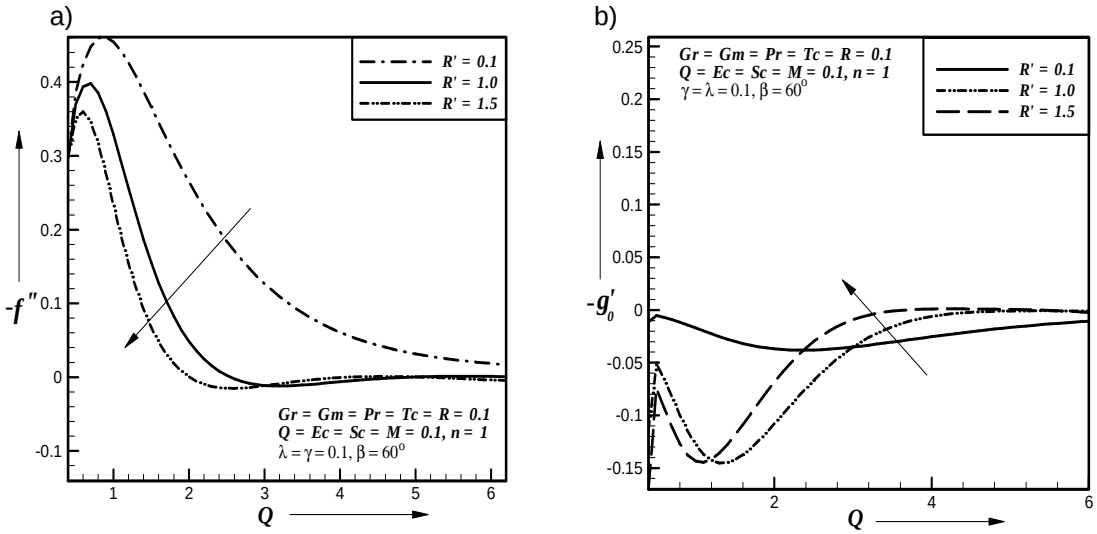

Fig. 12. Effect of rotational parameter on a) primary shear stress b) secondary shear stress

Figs. 13a and 13b represent the primary shear stress $(-f'')$ and secondary shear stress $(-g_0')$ which are plotted against heat source parameter (Q) for different values of porosity parameter. It is observed that the primary shear stress is decreases and secondary shear stress is increases with the increase of porosity parameter, where other parameters have the value $M = Gr = Gm = R' = Pr = Ec = Q = Tc = R = Sc = \lambda = 0.1, \beta = 60^0, n = 1$.

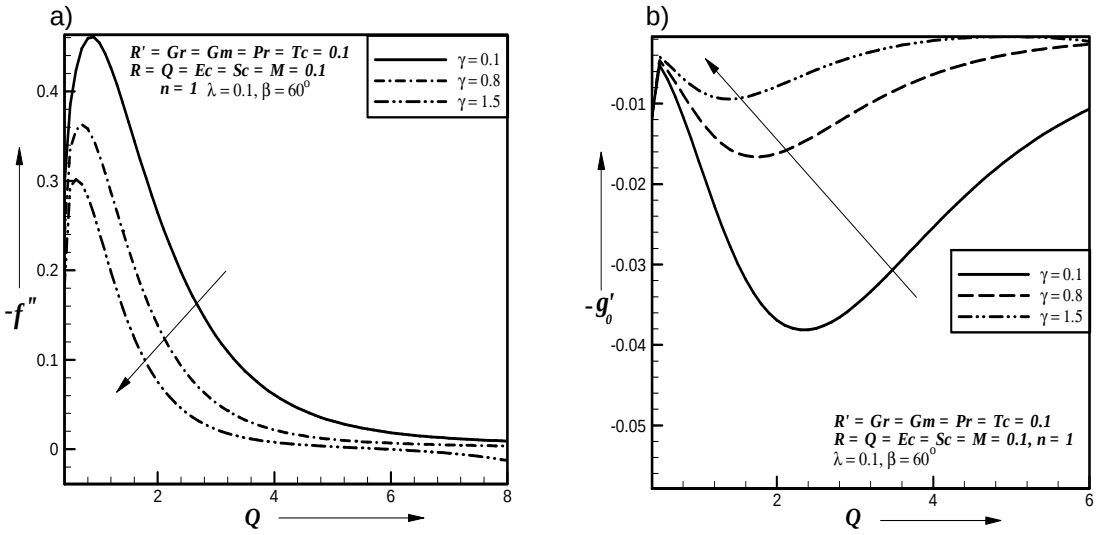

Fig. 13. Effect of porosity parameter on a) primary b) secondary shear stress

Fig. 14a represents the primary shear stress $(-f'')$ which is plotted against heat source parameter (Q) for different values of Grashof number. It is observed that the primary shear

stress is increases with the increase of Grashof number, where other parameters have the value $M = \gamma = Gm = R' = Pr = Ec = Q = Tc = R = Sc = \lambda = 0.1, \beta = 60^0, n = 1$.

Fig. 14b represents the primary shear stress $(-f'')$ which is plotted against heat source parameter (Q) for different values of modified Grashof number. It is observed that the primary shear stress is increases with the increase of modified Grashof number, where other parameters have the value $M = \gamma = Gr = R' = Pr = Ec = Q = Tc = R = Sc = \lambda = 0.1,\ \beta = 60^0,$ $n = 1$.

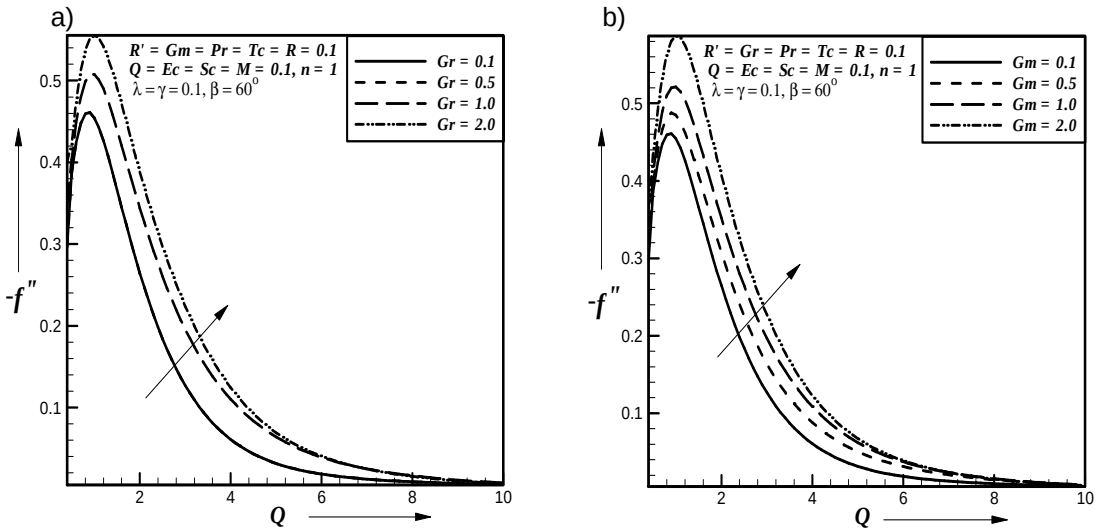

Fig. 14. Effect of a) Grashof number b) modified Grashof on primary shear stress

Fig. 15a represents the primary shear stress $(-f'')$ which is plotted against heat source parameter (Q) for different values of inclination angle. It is observed that the primary shear stress is decreases with the increase of inclination angle, where other parameters have the value $M = \gamma = Gm = Gr = R' = Pr = Ec = Q = Tc = R = Sc = \lambda = 0.1, n = 1$.

Fig. 15b represents the dimensionless heat transfer rate $(-\theta')$ which is plotted against Heat source parameter (Q) for different values of thermal conductivity parameter. It is observed that the heat transfer rate is increaseswith the increase of thermal conductivity parameter, where other parameters have the value $M = \gamma = Gm = Gr = R' = Pr = Ec = Q = R = Sc = 0.1,$ $\lambda = 0.1, \beta = 60^0, n = 1$.

Fig. 16a represents the dimensionless heat transfer rate $(-\theta')$ which is plotted against heat source parameter (Q) for different values of Prandtl number. It is observes that the heat transfer rate is decreased with the increase of Prandtl number, where other parameters have the value $M = \gamma = Gm = Gr = R' = Tc = Ec = Q = R = Sc = \lambda = 0.1, \beta = 60^0, n = 1$.

Fig. 16b represents the dimensionless heat transfer rate $(-\theta')$ which is plotted against Heat source parameter (Q) for different values of heat source parameter. It is observed that the

heat transfer rate is increases with the increase of heat source parameter, where other parameters have the value $M = \gamma = Gm = Gr = R' = Tc = Ec = Pr = R = Sc = \lambda = 0.1, \beta = 60^0$, $n = 1$.

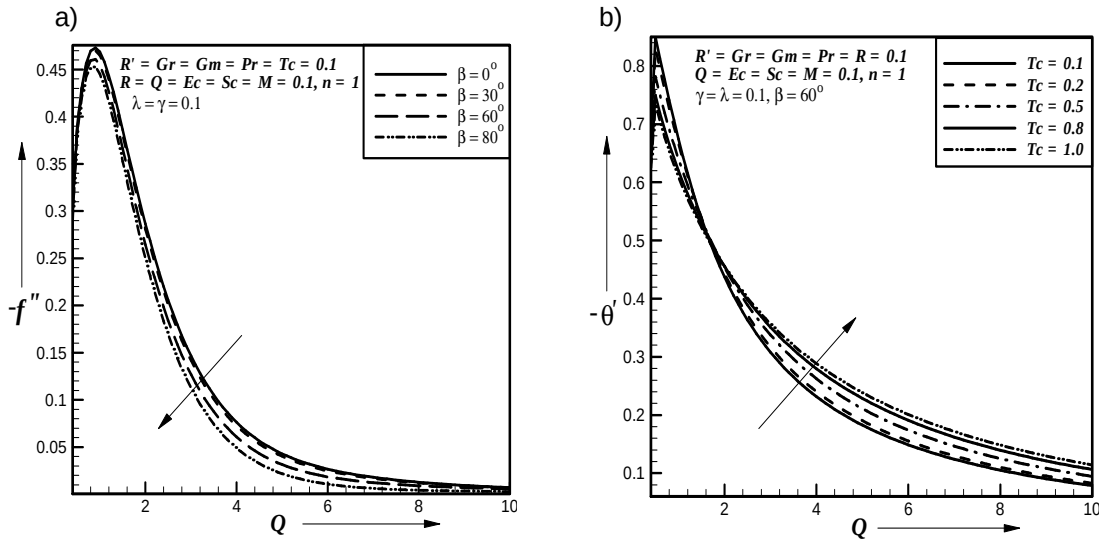

Fig. 15. Effect of a) inclination angle on primary shear stress b) thermal conductivity parameter on heat transfer rate

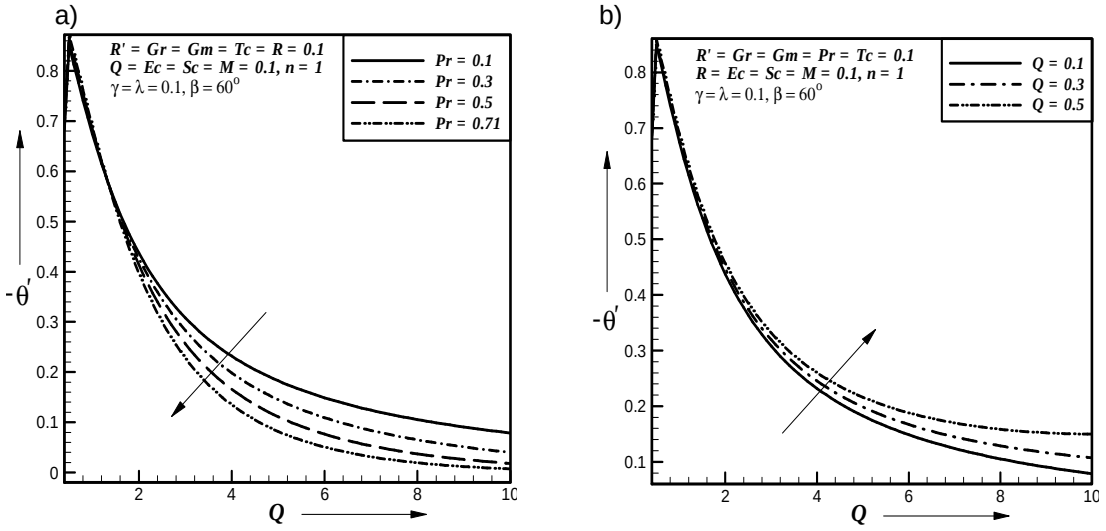

Fig. 16. Effect of a) Prandtl number b) heat source parameter on heat transfer rate

Fig. 17a represents the dimensionless heat transfer rate $(-\theta')$ which is plotted against heat source parameter (Q) for different values of Eckert number. It is observed that the heat transfer rate is increases with the increase of Eckert number, where other parameters have the value $M = \gamma = Gm = Gr = R' = Tc = Q = Pr = R = Sc = \lambda = 0.1, \beta = 60^0, n = 1$.

Fig. 17b represents the dimensionless heat transfer rate $(-\theta')$ which is plotted against heat source parameter (Q) for different values of radiation parameter. It is observed that the heat transfer rate is increases with the increase of radiation parameter, where other parameters have the value $M = \gamma = Gm = Gr = R' = Tc = Q = Pr = Ec = Sc = \lambda = 0.1,\ \beta = 60^0$, $n = 1$.

Fig. 18a represents the dimensionless mass transfer rate $(-\varphi')$ which is plotted against heat source parameter (Q) for different values of Schmidt number. It is observed that the mass transfer rate is decreases with the increase of Schmidt number, where other parameters have the value $M = \gamma = Gm = Gr = R' = Tc = Q = Pr = Ec = R = \lambda = 0.1,\ \beta = 60^0$, $n = 1$.

Fig. 18b represents the dimensionless mass transfer rate $(-\varphi')$ which is plotted against heat source parameter (Q) for different values of reaction parameter. It is observed that the mass transfer rate is decreases with the increase of reaction parameter, where other parameters have the value $M = \gamma = Gm = Gr = R' = Tc = Q = Pr = Ec = R = Sc = 0.1, \beta = 60^0$, $n = 1$.

Fig. 19 represents the dimensionless mass transfer rate $(-\varphi')$ which is plotted against heat source parameter (Q) for different values of order of chemical reaction. It is observed that the mass transfer rate is increases with the increase of order of chemical reaction, where other parameters have the value $M = \gamma = Gm = Gr = R' = Tc = Q = Pr = Ec = \lambda = R = Sc = 0.1$, $\beta = 60^0$.

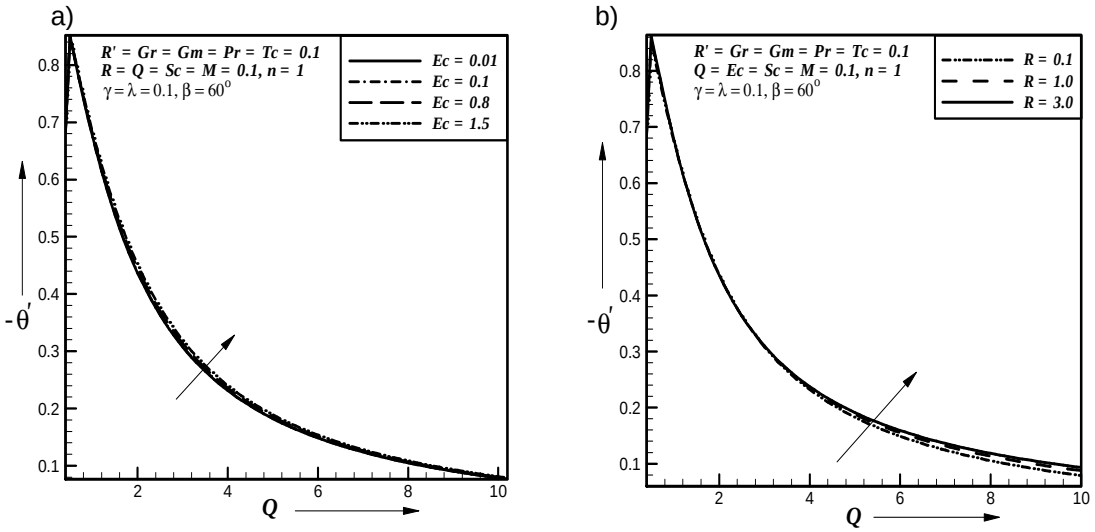

Fig. 17. Effect of a) Eckert number b) radiation parameter on heat transfer rate

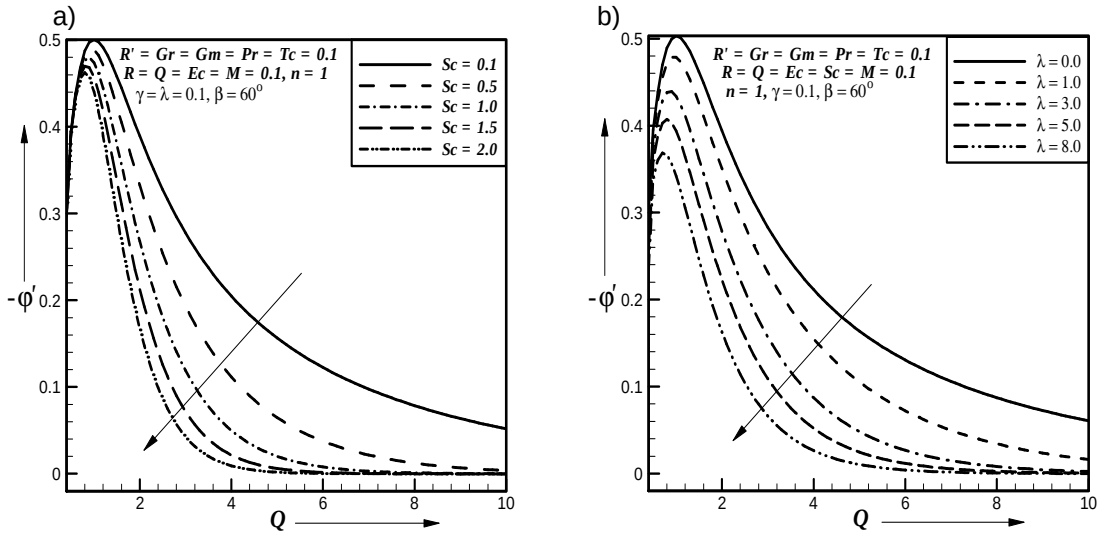

Fig. 18. Effect of a) Schmidt number b) reaction parameter on mass transfer rate

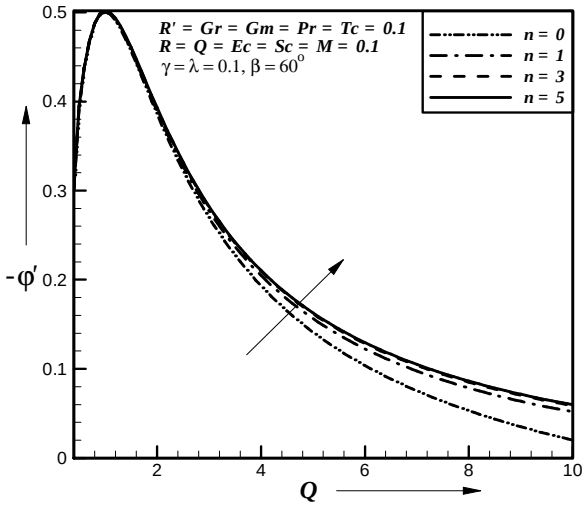

Fig. 19. Effect of order of chemical reaction on mass transfer rate

4. CONCLUSION

Laminar boundary layer flow past an inclined permeable plate of a rotating system with the influence of magnetic field, thermal radiation and chemical reaction has been investigated. The results are presented for various parameters. The velocity, temperature and concentration distributions for different parameters are shown graphically. The important findings of the investigation from graphical representation are listed below:

The primary velocity profiles are decreases due to increase of magnetic parameter where as the reverse effect is found for the secondary velocity profiles. Also the primary shear stress is decreases due to increase of magnetic parameter where as the reverse effect is found for secondary shear stress.

The primary velocity profiles and primary shear stress are decreases due to increase of rotational parameter where as the reverse effect is found for the secondary velocity profiles and secondary shear stress. Also the temperature and concentration boundary layer thickness are increases due to increase of rotational parameter.

The primary velocity profiles and primary shear stress are decreases due to increase of permeability of the porous medium where as the reverse effect is found for the secondary velocity profiles and secondary shear stress. Also the temperature and concentration boundary layer thickness are increases due to increase of permeability of the porous medium.

The primary velocity profiles and primary shear stress are decreases due to increase of inclination angle where as the reverse effect is found for the secondary velocity profiles.

The primary velocity profiles and primary shear stress are increases due to increase of Grashof number where as the reverse effect is found for the secondary velocity profiles. Also the temperature boundary layer thickness is decreases due to increase of Grashof number.

The primary velocity profiles and primary shear stress are increases due to increase of modified Grashof number where as the reverse effect is found for the secondary velocity profiles. Also the concentration boundary layer thickness is decreases due to increase of modified Grashof number.

The primary velocity profiles are increases due to increase of Prandtl number. The thermal boundary layer thickness as well as the heat transfer rate at the plate is decreases as the Prandtl number increases.

The heat transfer rate at the plate as well as the primary velocity is increases due to increase of Eckert number.

The temperature boundary layer thickness as well as the heat transfer rate at the plate is increases due to increase of thermal conductivity parameter.

The heat transfer rate at the plate is increases due to increase of heat source parameter.

The heat transfer rate at the plate is increases due to increase of radiation parameter.

The concentration boundary layer thickness as well as the mass transfer rate at the plate is decreases due to increase of Schmidt number.

The concentration boundary layer thickness as well as the mass transfer rate at the plate is decreases due to no reaction and destructive reaction.

The mass transfer rate at the plate is increases due to increase of order of chemical reaction.

COMPETING INTERESTS

Authors have declared that no competing interests exist.

REFERENCES

1. Bluman GW, Kumei S. Symmetries and Differential Equations. Springer-verlag: New York; 1989.
2. Helmy KA. MHD boundary layer equations for power law fluids with variable electric conductivity. Mechanica. 1995;30:187-200.
3. Pakdemirli M, Yurusoy M. Similarity transformations for partial differential equations. SIAM Review. 1998;40:96-101.

4. Kalpakides VK, Balassas KB. Symmetry groups and similarity solutions for a free convective boundary-layer problem. International Journal of Non-Linear Mechanics. 2004;39:1659-1670.
5. Makinde OD. Free convection flow with thermal radiation and mass transfer past moving vertical porous plate. International Communications in Heat and Mass Transfer. 2005 ;32:1411-1419.
6. Seddeek MA, Salem AM. Laminar mixed convection adjacent to vertical continuously stretching sheet with variable viscosity and variable thermal diffusivity. Heat and Mass Transfer. 2005;41:1048-1055.
7. Ibrahim FS, Elaiw AM, Bakr AA. Effect of the chemical reaction and radiation absorption on the unsteady MHD free convection flow past a semi infinite vertical permeable moving plate with heat source and suction. Communications in Nonlinear Science and Numerical Simulation. 2008; 13:1056-1066.
8. El-Kabeir SMM, El-Hakiem MA, Rashad. Lie group analysis of unsteady MHD three dimensional dimensional by natural convection from an inclined stretching surface saturated porous medium. Journal of Computational and Applied Mathematics. 2008;213:582-603.
9. Rajeswari R, Jothiram J, Nelson VK. Chemical Reaction, Heat and Mass Transfer on Nonlinear MHD Boundary Layer Flow through a Vertical Porous Surface in the Presence of Suction. Applied Mathematical Sciences. 2009;3:2469-2480.
10. Chandrakala P. Chemical Reaction Effects on MHD Flow Past An Impussively Started Semi-Infinite Vertical Plate. International Journal of Dynamics of Fluids. 2010;6:77-79.
11. Joneidi AA, Domairry G, Balaelahi M. Analytical treatment of MHD free convective flow and mass transfer over a stretching sheet with chemical reaction. Journal of the Taiwan Institute of Chemical Engineers. 2010;41: 35-43.
12. Muhaimin, Kandasamy R, Hashim I. Effect of chemical reaction, heat and mass transfer on nonlinear boundary layer past a porous shrinking sheet in the presence of suction. Nuclear Engineering and Design. 2010;240(5):933-939.
13. Rahman MM, Salahuddin KM. Study of hydromagnetic heat and mass transfer flow over an inclined heated surface with variable viscosity and electric conductivity. Communications in Nonlinear Science and Numerical Simulation. 2010;15:2073-2085.